Journal of Luminescence 145 (2014) 307–311

Contents lists available at ScienceDirect

Journal of Luminescence

journal homepage: www.elsevier.com/locate/jlumin

Plasma enhanced atomic layer deposition of magnesium oxide as a passivation layer for enhanced photoluminescence of ZnO nanowires

Jeong-Gyu Song [a], Jusang Park [a], Jaehong Yoon [a], Hwangje Woo [a], Kyungyong Ko [a], Taeyoon Lee [a], Sung-Hwan Hwang [b], Jae-Min Myoung [b], Keewon Kim [c], Youngman Jang [c], Kwangseok Kim [c], Hyungjun Kim [a,*]

[a] School of Electrical and Electronics Engineering, Yonsei University, 262 Seongsanno, Seodaemun-gu, Seoul, Republic of Korea
[b] Department of Materials Science and Engineering, Yonsei University, 262 Seongsanno, Seodaemun-gu, Seoul, Republic of Korea
[c] Samsung Advanced Institute of Technology (SAIT), Nongseo-dong, Giheung-gu, Yongin-si, Gyeonggi-do 446-712, Republic of Korea

ARTICLE INFO

Article history:
Received 15 May 2013
Received in revised form
12 July 2013
Accepted 31 July 2013
Available online 8 August 2013

Keywords:
Magnesium oxide
Atomic layer deposition
ZnO nanowires
Photoluminescence
Passivation

ABSTRACT

The growth characteristics and film properties of magnesium oxide (MgO) thin films fabricated by plasma enhanced atomic layer deposition (PE-ALD) and thermal ALD (Th-ALD) were comparatively investigated for passivation layer applications. For both processes, well-saturated growth characteristics were observed, with a higher saturated growth rate for Th-ALD. X-ray photoemission analysis showed that very high purity MgO film with virtually no carbon contamination was deposited by PE-ALD. X-ray diffraction and transmission electron microscopy analysis showed that the PE-ALD MgO thin films had a larger grain size than the Th-ALD MgO thin films and were predominantly (1 1 1) crystal orientation. The photoluminescence analysis showed enhanced luminescence properties of the ALD MgO shell/ZnO nanowires. In particular, PE-ALD MgO showed greater enhancement of the luminescence properties than Th-ALD MgO.

1. Introduction

Magnesium oxide (MgO) is widely used in various applications, such as in the protective layer in ac-plasma display panels (PDP) [1,2], as a tunneling barrier in magnetic tunneling junctions (MTJs) [3–7], and as a passivation layer in various optical and magnetic materials [8–12]. Recently, it was reported that the luminescence property of ZnO nanowires (NWs) near the ultra violet (UV) region is significantly enhanced by passivation with an MgO shell due to the reduced surface defect density of ZnO NWs [8–10]. The MgO shells were deposited by e-beam evaporation or hydrothermal growth. However, these processes have several limitations, such as poor conformality [9], non-uniformity, and difficulties in controlling thickness [8,10].

In this regard, atomic layer deposition (ALD) could be an attractive deposition technique, as it has excellent conformality for complicated nano-size structures and the ability to control thickness at the atomic scale [13]. There have been reports of thermal ALD (Th-ALD) of MgO thin films using various metal organic precursors, including bis(cyclopentadienyl)magnesium ($MgCp_2$), bis(ethylcyclopentadienyl)magnesium ($MgEtCp_2$), and magnesium 2,2,6,6-tetramethyl-3,5-heptadione ($Mg(thd)_2$) [14–16]. These reports have shown that the growth characteristics and film properties of ALD MgO are specifically dependent on the choice of precursor and growth conditions.

Plasma enhanced ALD (PE-ALD) could be an attractive alternative to conventional thermal ALD, which can produce high quality films at a low process temperature due to the high reactivity of radicals [17–19]. Notably, PE-ALD can reduce the interface and defect density between the substrate and deposited material, more so than Th-ALD [20]. Thus, it can be inferred that PE-ALD may be a promising technique for the deposition of passivation layers with improved optical properties and a low interface defect density for ZnO NW-based photonic devices. However, there have been no reports of PE-ALD MgO as a passivation layer for ZnO NWs or of PE-ALD MgO thin films. The growth characteristics and film properties of PE-ALD and Th-ALD MgO films fabricated using $MgCp_2$ as a Mg precursor were compared in this study. Furthermore, we studied the luminescence properties of ZnO NWs with Th- and PE-ALD MgO passivation layers.

2. Experimental

In this study, a commercial ALD chamber (Quros Plus 150™) with a loadlock chamber was used for PE-ALD analysis of MgO thin

* Corresponding author. Tel.: +82 2 21235773; fax: +82 2 3132879.
E-mail address: hyungjun@yonsei.ac.kr (H. Kim).

0022-2313/$ - see front matter © 2013 Elsevier B.V. All rights reserved.
http://dx.doi.org/10.1016/j.jlumin.2013.07.076

films. To produce adequate vapor pressure, the temperature of a bubbler containing $MgCp_2$ (solid) was maintained at 50 °C and vaporized $MgCp_2$ molecules were carried into the chamber by pure argon (99.999%) carrier gas. As a reactant, O_2 plasma was generated by an RF power generator. The O_2 flow and plasma power were fixed at 50 sccm and 100 W, respectively. An ALD cycle consisted of four steps: $MgCp_2$ precursor exposure (t_s), Ar purging (t_p), O_2 plasma reactant exposure (t_r), and another Ar purge (t_p). To purge the excess precursor molecules and by-products, Ar gas was used between each precursor and O_2 plasma exposure step. In the PE-ALD MgO process, t_s and t_r were systematically varied from 0.5 s to 5 s and from 1 s to 7 s, respectively, while t_p was fixed at 12 s.

For the Th-ALD MgO thin films, a homemade quartz tube furnace-type ALD chamber was employed. As with PE-ALD MgO, the $MgCp_2$ precursor was contained in a steel bubbler heated to 50 °C, and vaporized molecules were transported by the Ar carrier gas. Vaporized H_2O gas at room temperature was used as the reactant without an additional bubbling system. t_s, t_r, and t_p were fixed at 2 s, 1 s, and 12 s, respectively.

In both Th- and PE-ALD MgO processes, the deposition temperature (T_s) was 200 °C and the base pressure was 10^{-3} Torr. Si (0 0 1) and SiO_2(300 nm)/Si(0 0 1) were cleaned in an ultrasonic bath with acetone, IPA, and distilled water sequentially for 10 min each. Additionally, Si substrates were cleaned by dipping in a buffered oxide etchant (6:1) for 10 s, followed by a deionized (DI) water rinsing and N_2 blowing.

ZnO NWs were synthesized by a hydrothermal method. For this, a 125 nm thick ZnO seed layer was deposited using a Th-ALD ZnO process at T_s=150 °C and ZnO NWs were hydrothermally grown in 0.05 mol of zinc nitrate hexahydrate ($Zn(NO_3)_2 \cdot 6H_2O$) and a melted hexamethylenetetramine (HMT) aqueous solution for 180 min by maintaining the solvent temperature at 90 °C. Then, MgO shells were deposited on ZnO NWs by Th- or PE-ALD at T_s=200 °C.

The thickness of the MgO thin films was measured by spectroscopic ellipsometry. The microstructure of the films was analyzed by x-ray diffraction (XRD). The chemical composition and the impurity level were analyzed by x-ray photoelectron spectroscopy (XPS) using an Al kα monochromatic source of 1486.6 eV. The microstructures of the films were investigated by high-resolution cross-sectional transmission electron microscopy (HRTEM). The microstructure and optical properties of the ALD MgO shell/ZnO NWs were analyzed by scanning electron microscopy (SEM), transmission electron microscopy (TEM), and photoluminescence (PL) with a 325 nm excitation He–Cd laser at room temperature.

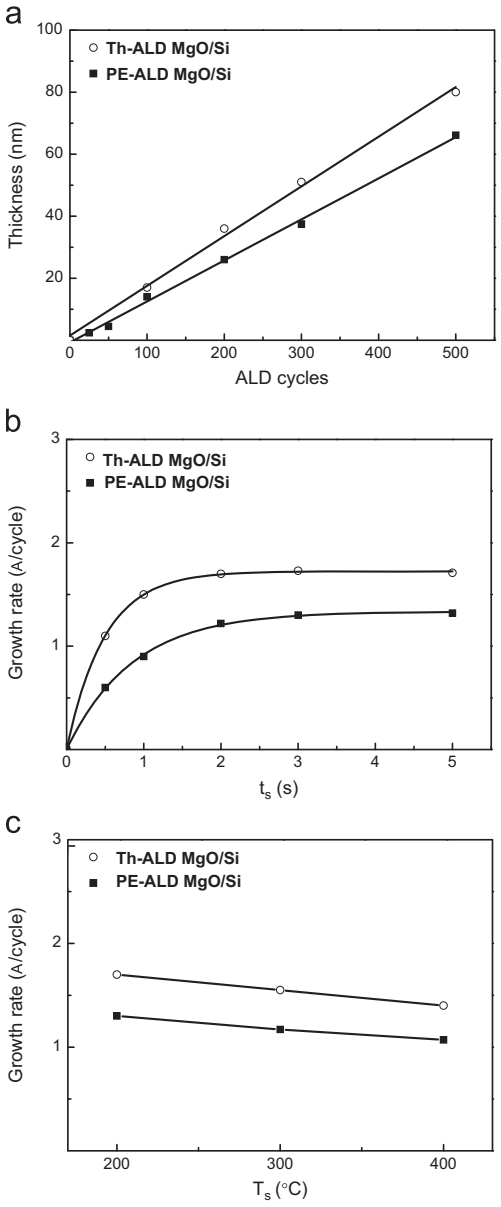

Fig. 1. Growth characteristics of ALD MgO thin films: (a) MgO thickness with increasing ALD cycles, (b) growth rate according to increasing source exposure time (t_s) and (c) deposition temperature (T_s).

3. Results and discussion

Fig. 1 shows the growth characteristics of the Th- and PE-ALD MgO thin films on Si substrates. The film thicknesses versus number of ALD cycles are plotted in Fig. 1(a). The growth rates of Th- and PE-ALD MgO were determined to be 1.7 and 1.3 Å/cycle from the linear fit of the plots, indicating that the growth rate of Th-ALD MgO is slightly higher than that of PE-ALD MgO. The reason for the higher growth rate of Th-ALD than that of the PE-ALD is not clear. However, in a previous report on the comparison between Th- and PE-ALD TiO_2, a similarly large growth rate for Th-ALD was reported [21]. The linear extrapolations of the plots passed though the origin for both processes, which indicated that both the ALD MgO processes lacked a significant nucleation delay. Fig. 1(b) shows the growth rates of Th- and PE-ALD MgO at various precursor exposure times, t_s. The growth rate of the Th-ALD MgO thin films was saturated at $t_s \geq 2$ s, while that of PE-ALD MgO was saturated at $t_s \geq 3$ s. These results indicated that $MgCp_2$ adsorption occurred with reasonable saturation in both the PE and Th-ALD processes. Fig. 1(c) shows the growth rates of Th- and PE-ALD MgO thin films according to growth temperature. The growth rates of Th- and PE-ALD MgO continuously decreased with increasing growth temperature between T_s=200 and 400 °C. The decrease in growth rates with increasing growth temperature is most likely related to a decrease in the number of reactive sites for precursor adsorption on the substrate and an increase of the Mg revaporization from the growth surface, as reported in previous reports [16,22].

Fig. 2 shows the XPS analysis results of the Th- and PE-ALD MgO thin films grown at T_s=200 °C after the surface was sputter cleaned by exposure to Ar. In the XPS spectra around the Mg core level shown in Fig. 2(a), clear Mg 2p peaks from Mg atoms bonded with oxygen are observed at 49.6 eV for both the Th- and PE-ALD MgO thin films [23]. Fig. 2(b) shows the O core levels in Th- and PE-ALD MgO thin films. In the Th-ALD MgO thin films, the O 1s peak is deconvoluted into three peaks located at 530.1 eV, 532 eV and 532.9 eV. The peak at the lowest energy was assigned to O–Mg

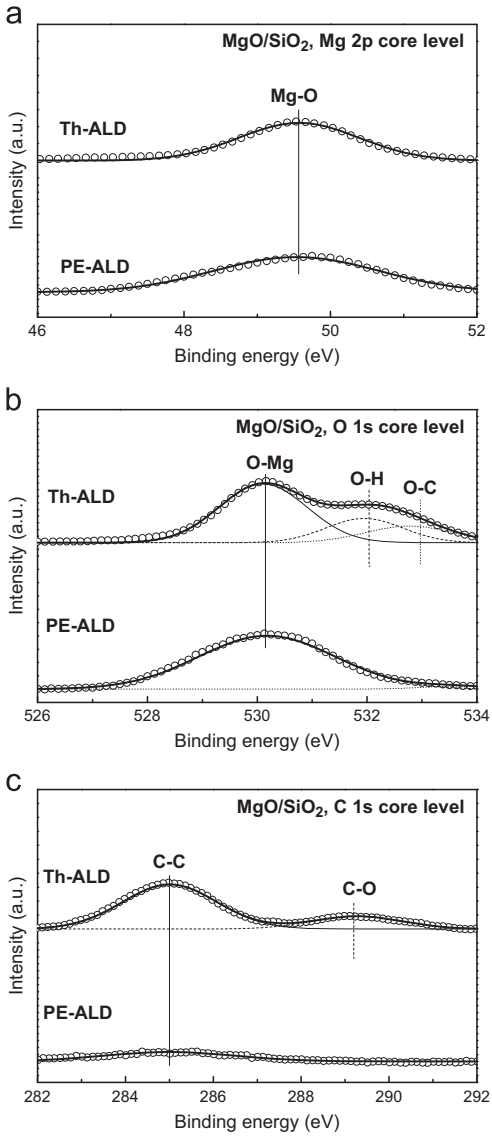

Fig. 2. The XPS results of Th- and PE-ALD MgO thin films: (a) Mg core level (b) O core level, and (c) C core levels.

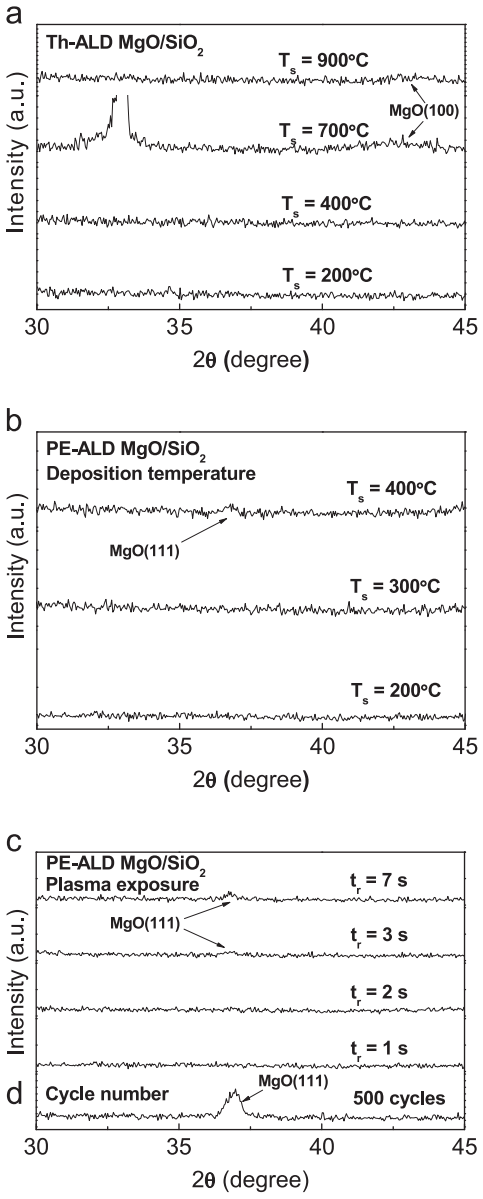

Fig. 3. The XRD spectra of MgO thin films on SiO_2 deposited by (a) Th-ALD MgO and PE-ALD MgO according to (b) deposition temperature, (c) plasma exposure time and (d) cycle number.

bonding, while the others were due to O–H and O–C bonding [24]. In contrast, the O 1 s core level XPS spectrum of PE-ALD MgO shows only one peak from O–Mg bonding. The observable H and C residue in the Th-ALD MgO thin films can be attributed to the Cp ligand tightly bonded *via* a π interaction to the Mg atom, resulting in hydrogen and carbon contamination during the Th-ALD of the MgO thin film [25]. Carbon impurity was also observed in the C 1s core level XPS spectrum (Fig. 2(c)). The carbon contamination was estimated to be about 3% for Th-ALD MgO thin films based on the XPS peak intensity, while carbon was under the detection limit of XPS in PE-ALD MgO. While there have been no reports regarding PE-ALD MgO using an $MgCp_2$ precursor, chemical reactions were analyzed with an *in situ* QMS study of PE-ALD using an oxygen radical and a $CoCp_2$ precursor to produce clean oxide films for Co oxide PE-ALD [25]. It was inferred that an analogous reaction for MgO PE-ALD may proceed through the following two reactions, $MgCp_2\,(s) \rightarrow MgCp_2\,(ads)$ and $MgCp_2\,(ads)+26O(g) \rightarrow MgO+10CO_2+5H_2O$, producing clean MgO films by PE-ALD.

Fig. 3 shows the XRD spectra of Th- and PE-ALD MgO thin films (200 cycles) on SiO_2 grown at different temperatures. As shown in Fig. 3(a), there is no clear diffraction peak at growth temperatures below 400 °C, indicating that the crystallinity of the film is poor. However, as deposition temperature increased over 700 °C, a broad but identifiable MgO (2 0 0) peak was observed at around 42.9°. A diffraction peak at 32.9°, which is observed at a growth temperature of 700 °C, is the Si (0 0 2) "ghost" reflection due to the Si substrate, and is not from the MgO thin film. In a previous report on Th-ALD MgO, the preferred orientation changed from (1 1 1) to (2 0 0) with increasing temperature above 700 °°C, which was suggested to be related to the grain shape and dissociation of the Mg precursor [26]. The present results showed a very weak (2 0 0) diffraction peak at high growth temperatures and no clear diffraction peak at lower growth temperatures, which is primarily due to the small thickness of the Th-ALD MgO (below 30 nm).

Fig. 3(b) shows the XRD spectra of PE-ALD MgO films grown from T_s=200 to 400 °C. For PE-ALD, the temperature range could not exceed 500 °C due to the limitations of the deposition chamber. At T_s=400 °C, in contrast to Th-ALD MgO, a small but clear diffraction peak is observed that decreases in intensity with decreasing growth temperature. Thus, although the preferred

(2 0 0) orientation was not achieved at growth temperatures below 400 °C, the use of plasma enables the crystallization of the very thin film. Then, the effect of plasma exposure on the microstructure was studied by changing the plasma exposure time. Fig. 3(c) shows the XRD spectra of the PE-ALD MgO thin films grown at various plasma exposure times (t_r) grown at T_s=200 °C for 200 cycles. While no diffraction peak was observed for $t_r \leq 2$ s, the MgO (1 1 1) peak was observed at longer plasma exposure times. Similar enhancement of the crystallinity by increasing the plasma exposure time was reported for PE-ALD of ZrO_2 [18]. In addition, a clear MgO (1 1 1) diffraction peak was observed by increasing the number of cycles to 500 cycles at t_r=7 s and T_s=200 °C in Fig. 3(d), which confirmed that the weak diffraction peak in the XRD spectra for MgO thin films grown for 200 cycles was due to the small thickness.

The microstructures of Th- and PE-ALD MgO thin films were further analyzed by HRTEM analysis. HRTEM images of Th- and PE-ALD MgO thin films deposited at a deposition temperature 200 °C (200 cycles) on SiO_2 substrates are shown in Fig. 4. Fig. 4 (a) shows that the Th-ALD MgO thin film was nanocrystalline, although no clear diffraction peak was observed by XRD. The grains, typically with a size smaller than 10 nm, appeared to have a random orientation. The PE-ALD MgO thin film deposited at t_r=7 s showed a larger grain size than the Th-ALD MgO thin film, which showed an apparent columnar structure as shown in Fig. 4(b).

Another quality to be noticed is the existence of an amorphous MgO layer in both images. It is well known that when ALD of oxide thin films is carried out on Si substrates, an amorphous interlayer is formed due to the oxidation of Si substrates [27,28]. However, since the MgO layers were deposited on SiO_2, not Si, these amorphous layers are probably not the SiO_2 interlayer. The thickness of the amorphous layer was greater for Th-ALD, approximately 4 nm, compared with that with PE-ALD, which was approximately 2 nm; this also suggested that these layers were not interlayers, which would be thicker for PE-ALD [28]. Thus, it was inferred that these thin amorphous layers were an MgO layer formed in an early stage of growth [29]. It was surmised that the MgO film was crystallized only after a certain "critical thickness" was deposited, especially on an amorphous substrate such as SiO_2. This critical film thickness was also observed in ALD TiO_2 thin films on the amorphous native SiO_2 formed Si substrate. In these reports, Th-ALD TiO_2 thin films formed an amorphous TiO_2 film until approximately 2–5 nm in thickness and crystallized above this critical thickness [30,31].

The PE-ALD MgO thin films were of higher quality with lower hydrogen and carbon impurities and a larger grain size than Th-ALD MgO thin films. Using Th- and PE-ALD MgO process, the performances of Th- and PE-ALD MgO as passivation layers for ZnO NWs were compared. Based on the growth rates shown in Fig. 1, 30 cycles of Th-ALD (40 cycles of PE-ALD MgO) were carried out on ZnO NWs to produce a 5-nm-thick MgO shell. Fig. 5 (a) shows an SEM image of a hydrothermally grown ZnO NWs array on a ZnO seed layer. ZnO NWs were uniformly aligned and have diameters ranging between 50 and 150 nm. The inset of Fig. 5 (a) shows a TEM image of Th-ALD MgO shell/ZnO NWs, showing a conformal MgO shell coating approximately 5 nm thick on the ZnO NWs. The PE-ALD MgO shell also showed good conformality, with a thickness of 5 nm (image not shown).

Fig. 5(b) shows the PL spectra of bare ZnO NWs and 5 nm thick Th- and PE-ALD MgO shell/ZnO NWs. The bare ZnO NWs PL

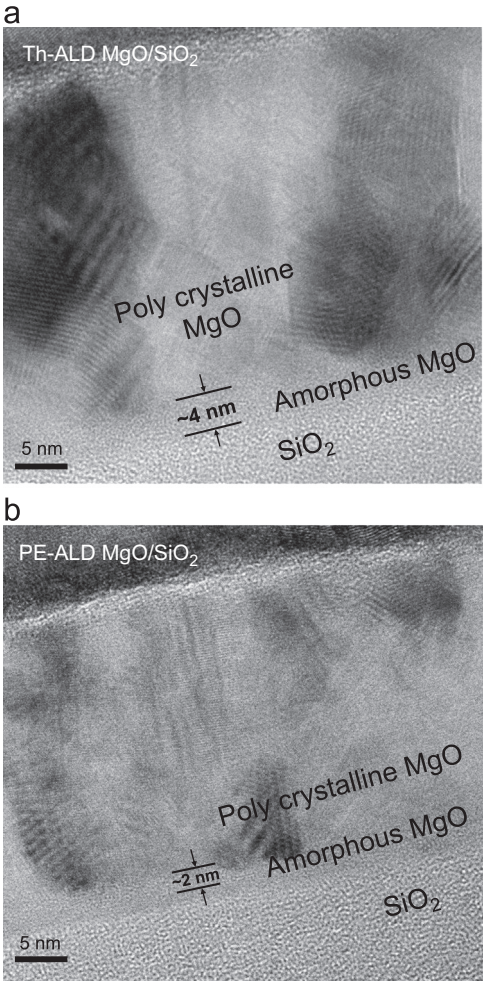

Fig. 4. The HRTEM images of (a) Th-ALD MgO and (b) PE-ALD MgO.

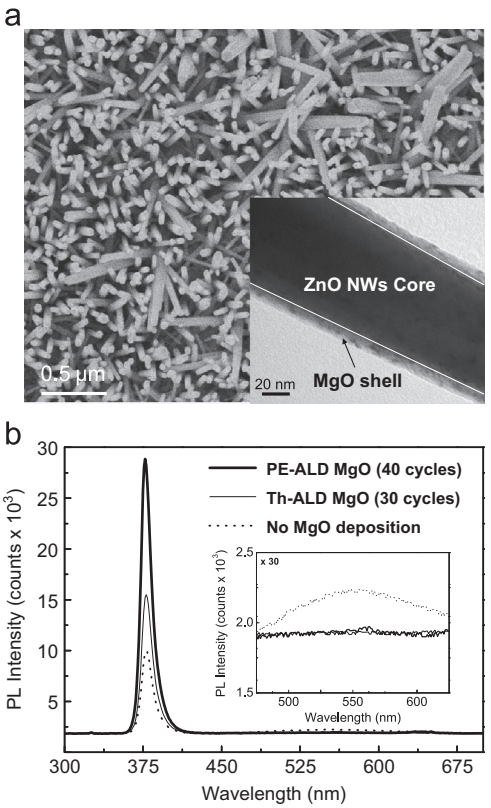

Fig. 5. (a) SEM image of bare ZnO NW array and (inset) TEM image of the Th-ALD MgO shell/ZnO NW and (b) PL spectra of the ZnO NWs with and without a Th- and PE-ALD MgO shell.

spectrum exhibited a dominant near-band-edge (NBE) emission at 377 nm, excitons-related recombination, and weak surface-mediated deep level (DL) traps emission at around 550 nm, which were ascribed to oxygen vacancies [8–10]. With the formation of an MgO shell with Th- and PE-ALD, the DL trap peak intensity decreased to noise level with increasing NBE peak intensity, as shown in the inset of Fig. 5(b). The intensity ratio of NBE to DL emission increased 1.5 times and 3 times for the Th- and PE-ALD MgO shell/ZnO NWs, which indicated that the PE-ALD MgO had a better passivation effect compared with Th-ALD MgO. Direct quantitative comparison with previous reports on the passivation effect of MgO coatings using other deposition processes, including the evaporation or the hydrothermal process, is difficult because the qualities of the ZnO NWs studies differed. However, the current results indicated that a very thin ALD MgO coating had at least a comparable passivation effect compared with other previously reported processes with larger thicknesses [8–10]. This enhanced PL intensity ratio by the MgO shell was attributed to a suppression of surface, nonradiative recombination and surface-mediated deep level traps of the ZnO NWs [8–10].

The improved passivation effect observed with the PE-ALD MgO shell/ZnO NWs over the Th-ALD MgO shell/ZnO NWs may be due to a smaller amount of hydroxyl species at the interface of the PE-ALD MgO shell/ZnO NWs. In a previous report, an impact of the hydroxyl species on the surface of ZnO NWs has been investigated that hydroxyl species on the surface of ZnO NWs playing a role as a donor surface states, and suppress UV luminescence by trapping a hole and hindering radiative recombination [32]. As shown in the XPS results of Th- and PE-ALD MgO thin films (Fig. 2), Th-ALD MgO thin films have a larger amount of hydroxyl species than the PE-ALD MgO. It was expected that the amount of hydroxyl bonding at the interface would be higher for the Th-ALD MgO, although the current XPS results showed otherwise. Additionally, other differences in film properties, such as the density, amount of contamination, surface roughness, crystallinity and interface trap density, cannot be excluded.

4. Conclusion

In this study, a comparative investigation of PE-ALD MgO and Th-ALD MgO thin films was conducted in the context of growth characteristics, chemical composition, microstructure, and applicability as a passivation layer. The thickness of the MgO films increased linearly with the number of cycles and the self-limited saturation of Th- and PE-ALD was observed above $t_s = 3$ s. The growth rate of the Th-ALD MgO thin films was slightly higher than that of the PE-ALD MgO thin films. High-purity MgO thin films with a comparatively negligible amount of carbon for Th-ALD MgO thin films were deposited by PE-ALD. The MgO thin films that were deposited on SiO_2 substrates by PE-ALD had a larger crystal grain than the Th-ALD MgO thin films and (1 1 1) orientation on SiO_2 substrates. Using Th- and PE-ALD MgO processes, it was confirmed that the PE-ALD MgO thin film has a better passivation effect for ZnO NWs compared with Th-ALD MgO thin films. As a result, PE-ALD MgO thin film has better properties than Th-ALD MgO thin film in terms of film quality and applicability as a passivation layer for ZnO NWs.

Acknowledgments

This work was supported by the Industrial Strategic technology development program (10041926, development of high density plasma technologies for thin film deposition of nanoscale semiconductor and flexible display processing) funded by the Ministry of Knowledge Economy (MKE, Korea).

References

[1] J. Hae-Yoon, L. Tae-Ho, K. Ohyung, C. Hee-Woon, S.O. Steinmuller, J. Janek, W. Ki-Woong, IEEE Trans. Electron Devices 31 (2010) 686.
[2] T. Jüstel, H. Nikol, Adv. Mater. 12 (2000) 527.
[3] C. Chappert, A. Fert, F.N. Van Dau, Nat. Mater. 6 (2007) 813.
[4] J.S. Moodera, L.R. Kinder, T.M. Wong, R. Meservey, Phys. Rev. Lett. 74 (1995) 3273.
[5] H. Kubota, A. Fukushima, K. Yakushiji, T. Nagahama, S. Yuasa, K. Ando, H. Maehara, Y. Nagamine, K. Tsunekawa, D.D. Djayaprawira, N. Watanabe, Y. Suzuki, Nat. Phys. 4 (2008) 37.
[6] S.S.P. Parkin, C. Kaiser, A. Panchula, P.M. Rice, B. Hughes, M. Samant, S.-H. Yang, Nat. Mater. 3 (2004) 862.
[7] S. Yuasa, T. Nagahama, A. Fukushima, Y. Suzuki, K. Ando, Nat. Mater. 3 (2004) 868.
[8] H.Y. Yang, S.F. Yu, G.P. Li, T. Wu, Opt. Express 18 (2010) 13647.
[9] C.Y. Liu, H.Y. Xu, J.G. Ma, X.H. Li, X.T. Zhang, Y.C. Liu, R. Mu, Appl. Phys. Lett. 99 (2011) 063113.
[10] C. Jin, H. Kim, C. Hong, J. Lee, C. Lee, Curr. Appl. Phys. 11 (2011) S60.
[11] Y.J. Zeng, Z.Z. Ye, F. Liu, D.Y. Li, Y.F. Lu, W. Jaeger, H.P. He, L.P. Zhu, J.Y. Huang, B. H. Zhao, Cryst. Growth Des. 9 (2008) 263.
[12] J. Kim, C. Rong, Y. Lee, J.P. Liu, S. Sun, Chem. Mater. 20 (2008) 7242.
[13] H. Kim, H.-B.-R. Lee, W.J. Maeng, Thin Solid Films 517 (2009) 2563.
[14] R. Huang, A.H. Kitai, Appl. Phys. Lett. 61 (1992) 1450.
[15] B.B. Burton, D.N. Goldstein, S.M. George, J. Phys. Chem. C 113 (2009) 1939.
[16] M. Putkonen, T. Sajavaara, L. Niinisto, J. Mater. Chem. 10 (2000) 1857.
[17] K. Hyungjun, Thin Solid Films 519 (2011) 6639.
[18] S.J. Yun, J.W. Lim, J.H. Lee, Electrochem. Solid-State Lett. 8 (2005) F47.
[19] J.W. Lim, S.J. Yun, Electrochem. Solid-State Lett. 7 (2004) F45.
[20] W.-H. Kim, W. Maeng, K.-J. Moon, J.-M. Myoung, H. Kim, Thin Solid Films 519 (2010) 362.
[21] Q. Xie, J. Musschoot, D. Deduytsche, R.L. Van Meirhaeghe, C. Detavernier, S. Van den Berghe, Y.-L. Jiang, G.-P. Ru, B.-Z. Li, X.-P. Qu, J. Electrochem. Soc. 155 (2008) H688.
[22] Y. Ohba, Y. Nishikawa, C. Nozaki, H. Sugawara, T. Nakanisi, J. Cryst. Growth 93 (1988) 613.
[23] S. Ardizzone, C.L. Bianchi, M. Fadoni, B. Vercelli, Appl. Surf. Sci. 119 (1997) 253.
[24] H.-L. Lu, S.-J. Ding, D.W. Zhang, Electrochem. Solid-State Lett. 13 (2010) G25.
[25] M.E. Donders, H.C.M. Knoops, M.C.M. van de Sanden, W.M.M. Kessels, P.H. L. Notten, J. Electrochem. Soc. 158 (2011) G92.
[26] R. Huang, A.H. Kitai, J. Mater. Sci. Lett. 12 (1993) 1444.
[27] J. Kim, S. Kim, H. Jeon, M.H. Cho, K.B. Chung, C. Bae, Appl. Phys. Lett. 87 (2005) 053103.
[28] P.K. Park, J.-S. Roh, B.H. Choi, S.-W. Kang, Electrochem. Solid-State Lett. 9 (2006) F34.
[29] V. Miikkulainen, M. Leskela, M. Ritala, R.L. Puurunen, J. Appl. Phys. 113 (2013) 021101.
[30] D.R.G. Mitchell, D.J. Attard, G. Triani, Thin Solid Films 441 (2003) 85.
[31] W.D. Kim, G.W. Hwang, O.S. Kwon, S.K. Kim, M. Cho, D.S. Jeong, S.W. Lee, M. H. Seo, C.S. Hwang, Y.-S. Min, J. Electrochem. Soc. 152 (2005) C552.
[32] W.Z. Liu, H.Y. Xu, J.G. Ma, C.Y. Liu, Y.X. Liu, Y.C. Liu, Appl. Phys. Lett. 100 (2012) 203101.